J. Min. Metall. Sect. B-Metall. 58 (2) (2022) 203 - 218

Journal of Mining and Metallurgy, Section B: Metallurgy

MICROSTRUCTURES AND TENSILE PROPERTIES OF Mg-2Zn-0.8Sr-0.2Ca ALLOY EXTRUDED AT RELATIVELY SLOW SPEED AND LOW TEMPERATURE

A. Yang [a], K.-B. Nie [a, b, *], K.-K. Deng [a, b], J.-G. Han [a], T. Xiao [c], X.-Z. Han [c,]**

[a] College of Materials Science and Engineering, Taiyuan University of Technology, Taiyuan, PR China
[b] Shanxi Key Laboratory of Advanced Magnesium-based Materials, Taiyuan University of Technology, Taiyuan, PR China
[c] Beijing Institute of Spacecraft System Engineering, Beijing, PR China

(Received 25 March 2021; Accepted 11 April 2022)

Abstract

In this work, a new Mg-2Zn-0.8Sr-0.2Ca alloy with low content of alloying elements was subjected to extrusion at relatively low-temperatures (240 and 200°C) and slow-speed (1.0 mm/s and 0.1 mm/s). The average size and volume fraction of recrystallized grains in the extruded Mg-2Zn-0.8Sr-0.2Ca alloy gradually decreased with the reduction in extrusion rate or extrusion temperature. Some broken second phases including $Ca_2Mg_6Zn_3$ and $Mg_{17}Sr_2$ appeared in the extruded Mg-2Zn-0.8Sr-0.2Ca alloy along with some precipitated nano-sized $MgZn_2$ phases. The volume fraction of $MgZn_2$ phases gradually in the alloy increased as extrusion rate or temperature decreased. High performance with yield strength of 393.1 MPa, ultimate tensile strength of 418.4 MPa and the elongation of 5.7% was obtained in the Mg-2Zn-0.8Sr-0.2Ca alloy extruded at 200°C & 0.1 mm/s. The main strengthening mechanisms could be attributed to grain-boundary strengthening, dislocation strengthening, precipitation strengthening, which were related to the change in grain size, second phases and basal texture intensity for the extruded Mg-2Zn-0.8Sr-0.2Ca alloy.

Keywords: *Mg-2Zn-0.8Sr-0.2Ca alloy; Extrusion; Microstructure; Texture; Mechanical properties*

1. Introduction

Lightweight magnesium and its alloys are of great potential for application in aerospace engineering, vehicle transportation, electronic and biomedical devices, because of their low density, high specific strength and specific stiffness and good biocompatibility [1-3]. However, the strength of pure magnesium is very low, which significantly restricts the application range. The addition of alloying elements to magnesium can effectively optimize the microstructure and improve its mechanical properties [4]. Among many magnesium alloy series, the Mg-Zn series alloys have become the most popular magnesium alloy series due to their good aging strengthening effect, corrosion resistance and low cost [5, 6]. The solid solubility of Zn in Mg was 6.2 wt.% at 613K, which decreased as the temperature decreased [7]. Meanwhile, previous studies have shown that Zn and Mg mainly exist as second phase compounds such as MgZn phase, $MgZn_2$ phase, Mg_2Zn_3 phase or Mg_4Zn_7 phase [7, 8], leading to significant second phase strengthening. However, the addition of the Zn element also has some adverse effects such as shrinkage porosity and hot cracking, reducing the casting properties of Mg-Zn binary alloys. In this situation, a third alloying element is required to improve casting defects and achieve excellent properties for the Mg-Zn binary alloys. Compared with high-cost RE elements, Sr is conducive to improving the thermal crack resistance of magnesium alloys. The trace addition (<1.0 wt.%) of Sr can also refine the microstructure of magnesium alloys and improve the mechanical properties [9]. From a thermodynamic point of view, the addition of Sr accelerates the formation of supercooling and refines the grains [10]. Moreover, Sr is a surface-active element, and an adsorption film containing Sr can be formed on the interface, resulting in a decrease in the grain growth rate [11]. Guan [12] et al. studied the microstructure and mechanical properties of a Mg-4.0Zn-1.0Sr (wt.%) alloy, and found that the ultimate tensile strength (UTS) was 270 MPa with the elongation (EL) of 12.8 % after rolling followed aging treatment. In addition, some scholars have studied the Mg-Zn alloys through composite addition of Sr and Ca

Corresponding author: niekaibo2015@163.com [*]; xiuzhuhan@163.com [**];

https://doi.org/10.2298/JMMB210325004Y

elements. Ding [13] et al. reported that Ca could optimize the microstructure more effectively than Sr in the as-cast and rolled Mg-Zn alloys, and the best comprehensive mechanical properties including a UTS of 317 MPa, yield strength (YS) of 235 MPa and EL of 24% were achieved in the rolled Mg-5Zn-0.4Ca-0.2Sr alloy. Furthermore, as an inexpensive and ideal alloying element, the Ca element can not only refine grains [14] but also ameliorate the oxidation resistance and corrosion resistance [15]. Previous studies regarding on Mg-Zn-Sr or Mg-Zn-Sr-Ca alloys mainly focused on high Zn concentration (>3 wt.%) [9, 12, 13]. However, there are a few related research reports in terms of the microalloying Mg-Zn-Sr-Ca alloys with low Zn concentration (< 3wt.%), especially with low Ca concentration (< 0.5wt.%) and low Sr concentration (< 1wt.%). Therefore, in this current work, the new Mg-2Zn-0.8Sr-0.2Ca alloy was designed and prepared.

Meanwhile, thermal deformation such as extrusion [16, 17], rolling [13, 18] and forging [19, 20], can not only eliminate casting defects such as porosity in as-cast magnesium alloys but also refine the grains and optimize the microstructure of magnesium alloys. Extrusion is the most efficient and straightforward way to deform the magnesium alloys. Tong [21] et al. studied the indirect-extrusion Mg-5.3Zn-0.6Ca alloy and showed that as the extrusion rate rised, the volume fraction and the grain size of the dynamic recrystallization (DRX) increased, the texture was significantly weakened, and the YS was substantially reduced. Du [22] et al. performed hot extrusion on a Mg-4.50Zn-1.13Ca (wt.%) alloy at different temperatures. There were a lot of deformed microstructures when the alloy was extruded at 300°C, and the basal texture was strong, leading to high strength and low plasticity. In contrast, when the alloy was extruded at 350°C, the DRX was relatively complete, the basal texture was weak, the strength decreased and the plasticity increased. Thus, optimal extrusion parameters are the key to achieve a balance between strength and plasticity. However, the influence of extrusion temperature and extrusion rate on the present Mg-2Zn-0.8Sr-0.2Ca alloy is yet to be explored based on existing literature search. In this work, the new Mg-2Zn-0.8Sr-0.2Ca alloy with low content of alloying elements was subjected to extrusion at relatively low-temperatures (240 and 200°C) and slow-speed (1.0 mm/s and 0.1 mm/s). The microstructure, texture and mechanical properties of extruded Mg-2Zn-0.8Sr-0.2Ca alloy have been investigated to develop a low-cost, high-strength Mg-Zn-Sr-Ca wrought magnesium alloy.

2. Experimental procedures

2.1. The preparation of Mg-2Zn-0.8Sr-0.2Ca alloy

To prepare the Mg-2Zn-0.8Sr-0.2Ca alloy, pure Mg (99.99%), pure Zn (99.99%), pure Ca (99.5%) and Mg-20 wt.% Sr master alloy were melted in the stainless steel crucibles using a resistance furnace under the protection of CO_2 and SF_6 (the volume ratio of CO_2 and 0.5% SF_6 is 40:1) mixed protective gas. Mg-20 wt.% Sr, pure Zn, and pure Ca were added to the molten magnesium at 750°C. After holding for 20 min, the melt was poured into a stainless steel mold preheated to 250°C to obtain a round bar ingot of Φ 40 mm × h 200 mm.

2.2. The extrusion of Mg-2Zn-0.8Sr-0.2Ca alloy

The Mg-2Zn-0.8Sr-0.2Ca alloy ingot was processed into equal volume blocks of Φ 40 mm × h 45 mm by wire cutting machine, and then homogenized at 320°C for 8 h, followed at 400°C for 12h, and subsequently, the samples were quickly water-cooled. The samples were maintained at the corresponding extrusion temperature for 30 min. The extrusion temperature was set at 200°C at an indenter speed of 1.0 mm/s and 0.1 mm/s, or the extrusion speed was fixed at 0.1 mm/s at the extrusion temperature of 200°C and 240°C with an extrusion ratio of 16:1. Finally, according to the hot extrusion process conditions, the extruded samples were defined as 200°C&1.0 mm/s, 200°C&0.1 mm/s, and 240°C&0.1 mm/s.

2.3. The microstructure characterization of Mg-2Zn-0.8Sr-0.2Ca alloy

1,500 and 4,000 grit sandpapers were used to grind samples obtained along the extrusion direction (ED) of extruded bars. The prepared extruded samples were etched with a mixed corrosive of oxalic acid and nitric acid alcohol (volume ratio 3:2). The microstructure of samples was observed by a light microscope (4XC). A field emission scanning electron microscope (FESEM, Mira 3XMU) equipped with energy dispersive spectroscopy (EDS, Oxford) and electron backscatter diffraction (EBSD) was used to characterize the microstructure of Mg-2Zn-0.8Sr-0.2Ca alloy. The samples ground with 1,500 and 4,000 grit sandpapers were electropolished with 5% perchloric acid for 60 s at -30°C, and the electrolytic current was 0.2 A. During the test, the samples were tilted 70°, the distance between the samples and the table was 15 mm, the scanning voltage was 20 kV, and the scanning step was 0.1 μm. The X-ray diffraction (XRD) analysis was carried out with a scanning 2θ angles of 10°-90° and a scanning speed of 2°/min for phase identification. A transmission electron microscope (TEM, JEM-2100HR) was used for further microstructure characterization. The volume fractions of the dynamic recrystallized (DRXed) regions and the DRXed grain sizes were depicted

using the Photoshop software. Then the volume fractions of the DRXed regions and the average DRXed grain size were computed by the Image-Pro Plus (IPP) software. The corresponding statistical results were put into Origin software, and the distribution of grain size could be obtained.

2.4. Tensile test at room-temperature

Flat dog-bone tensile samples with a cross-sectional area of 10 mm × 2 mm and a gauge length of 25 mm were cut from extruded bars parallel to the ED by the wire cutting machine, and the samples were ground to remove the cutting marks. The room temperature tensile test was implemented on the Instron Series 3369 testing equipment. An extensometer with the gauge length of 25 mm was used to measure the strain, and the test displacement rate was 0.5 mm min^{-1}. To ensure the accuracy of the results, three samples were performed for each process condition.

3. Results and discussions

3.1. Microstructures of as-extruded Mg-2Zn-0.8Sr-0.2Ca alloy

Figure 1 shows the light microscope images of Mg-2Zn-0.8Sr-0.2Ca alloys extruded at different extrusion conditions. Compared with the as-cast Mg-2Zn-0.8Sr-0.2Ca alloy [23], the grain sizes of the Mg-2Zn-0.8Sr-0.2Ca alloys after hot extrusion were significantly refined by DRX. When the extrusion parameter was 200 °C&1.0 mm/s, nearly fully DRXed microstructure appeared in the alloy with a volume fraction of DRX (V_{DRX}) of 94%. As the extrusion speed declined to 0.1 mm/s at 200 °C, the DRX degree was significantly reduced and the V_{DRX} was 58%, while a large number of twins could be observed. As the extrusion temperature increased to 240 °C at 0.1 mm/s, the V_{DRX} increased to 76%. Further, the statistical results of the grain size using the IPP software showed that average DRXed grains sizes (dDRX) at 200 °C&1.0 mm/s, 200 °C&0.1 mm/s and 240 °C&0.1 mm/s were 1.36 μm, 0.53 μm, and 0.76 μm, respectively. SEM images at high magnification were used to analyze the compositions of the second phases of the extruded Mg-2Zn-0.8Sr-0.2Ca alloys (Figure 2). Compared with the as-cast Mg-2Zn-0.8Sr-0.2Ca alloy [23], some secondary phases were broken after extrusion (Figure 2(a)(b)(c)). EDS results demonstrate that the broken secondary phases contain Mg, Zn, Sr, and Ca elements. Combining the corresponding XRD patterns of Mg-2Zn-0.8Sr-0.2Ca alloys in Figure 3, these fragmented secondary phases were confirmed to be $Ca_2Mg_6Zn_3$ and $Mg_{17}Sr_2$. Besides, at higher magnification (Figure 2(d)(e)(f)), some precipitates appeared in the extruded Mg-2Zn-0.8Sr-0.2Ca alloys. Besides, the broadening of the XRD peaks were calculated and found that the high-angle diffraction peaks of the α-Mg matrix were significantly enhanced with increasing extrusion temperature or extrusion rate, which may be related to the solubility of Zn atoms in the matrix [17]. EDS results (Table 1) for Figure 2(d)(e)(f) (marked with yellow arrows A-F) indicate the precipitated phases were Mg-Zn phases. According to the XRD patterns in Figure 3, these precipitated phases were considered as $MgZn_2$ phases, which was consistent with previous investigations on the extruded Mg-4Zn-0.5Ca alloys [16].

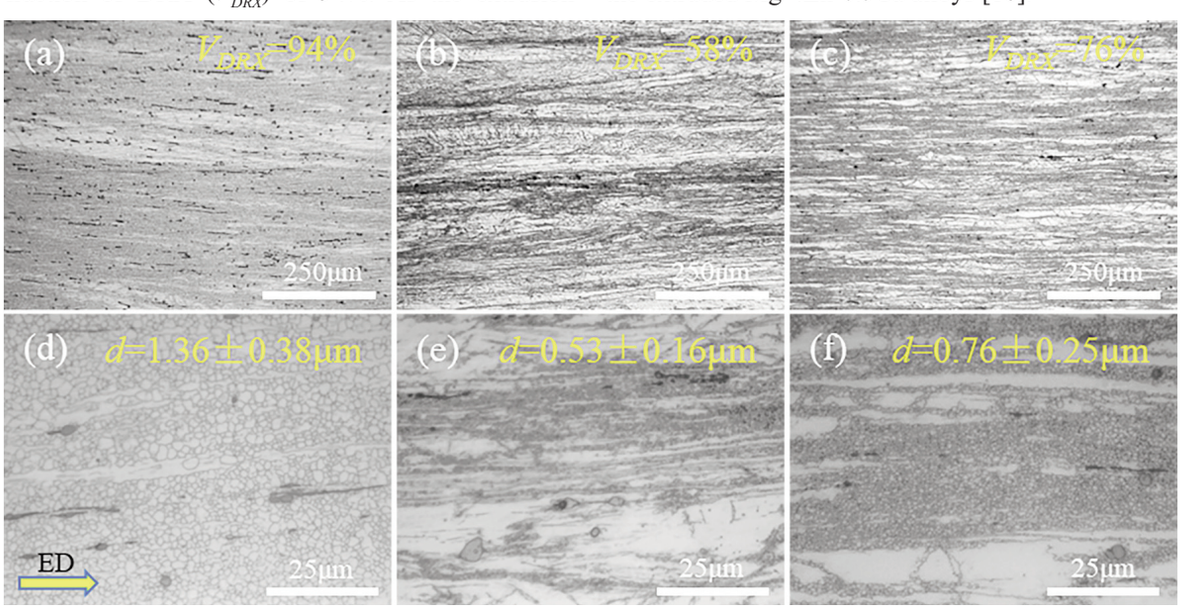

Figure 1. *The light microscope images of Mg-2Zn-0.8Sr-0.2Ca alloys extruded at different extrusion parameters: (a)(d) 200°C&1.0mm/s, (b)(e) 200°C&0.1mm/s and (c)(f) 240°C&0.1mm/s*

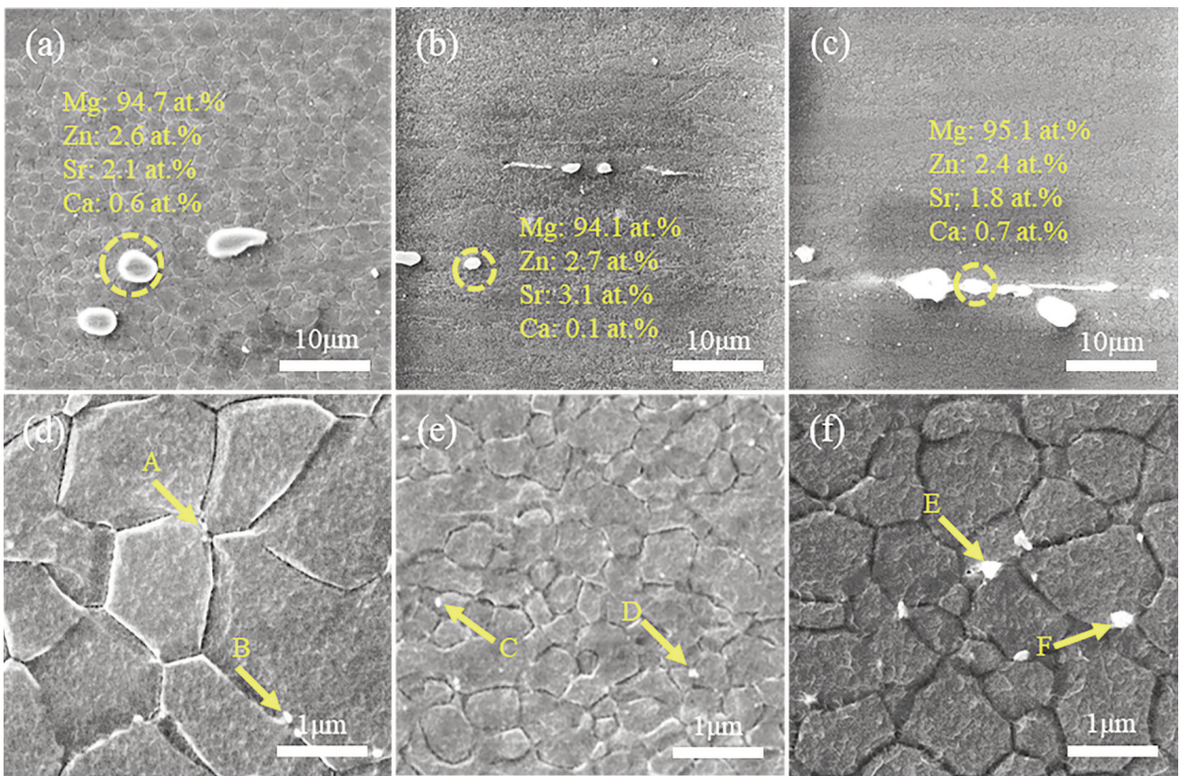

Figure 2. *SEM images of Mg-2Zn-0.8Sr-0.2Ca alloys extruded at different extrusion parameters: (a)(d) 200°C&1.0mm/s, (b)(e) 200°C&0.1mm/s and (c)(f) 240°C&0.1mm/s*

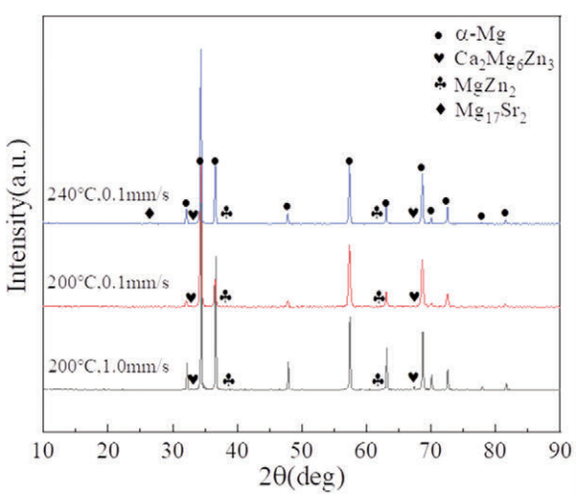

Figure 3. *XRD patterns of Mg-2Zn-0.8Sr-0.2Ca alloys extruded at different extrusion parameters*

The variation in the extrusion parameters such as extrusion ratio, extrusion rate and extrusion temperature can cause significant change to the values of d_{DRX}. Due to the extrusion ratio for the present Mg-2Zn-0.8Sr-0.2Ca alloy was set as 16:1, the $\bar{d}_{DRX}$ could be depicted by the following Zener-Hollomon (Z) parameter [16, 24]:

$$Z = \dot{\varepsilon}\exp\left(\frac{Q}{RT}\right) \quad (1)$$

Table 1. *EDS analysis of the as-extruded Mg-2Zn-0.8Sr-0.2Ca alloys in at. %*

Positions	Elements (at. %)				Possible phase
	Mg	Zn	Sr	Ca	
A	98.6	1.4	0.0	0.0	$MgZn_2$
B	99.5	0.5	0.0	0.0	$MgZn_2$
C	98.8	1.2	0.0	0.0	$MgZn_2$
D	99.3	0.7	0.0	0.0	$MgZn_2$
E	98.7	1.3	0.0	0.0	$MgZn_2$
F	99.1	0.9	0.0	0.0	$MgZn_2$

$$\bar{d}_{DRX} = AZ^{-n} \quad (2)$$

where $\dot{\varepsilon}$ means the extrusion strain rate, Q means the activation energy related to the lattice diffusion of the magnesium alloy, R means the gas constant and T means the deformation temperature, $\bar{d}_{DRX}$ means the average grain size of DRXed grains, A means a definite value related to the material, n means the power-law exponent. According to Eq. (1) and (2), when the $\dot{\varepsilon}$ is a constant, as the extrusion temperature increases, the Z value gradually decreases, and $\bar{d}_{DRX}$ gradually increases, which is consistent with the $\bar{d}_{DRX}$ of the present Mg-2Zn-

0.8Sr-0.2Ca alloys extruded at 200 °C&0.1 mm/s and 240 °C&0.1 mm/s. Further, according to the Arrhenius law [25]: $D = D_0 \exp\left(-\frac{Q}{RT}\right)$, the temperature can intensively affect the diffusion ability of atoms. As the temperature increases, the diffusion coefficient D increases. Therefore, as the extrusion temperature increases, Zn, Sr, and Ca atoms can be easy to diffuse. The number of heterogeneous nucleation sites increases in the magnesium matrix, leading to an increase in V_{DRX}. However, the larger the diffusion coefficient D, the easier it is for the grain boundaries to migrate [26], thus resulting in the growth of DRXed grains of Mg-2Zn-0.8Sr-0.2Ca alloys.

Additionally, the can be expressed by the following equation [24, 27, 28]:

$$\dot{\varepsilon} = \frac{6D_B^2 V_R \ln ER}{D_B^3 - D_E^3} \quad (3)$$

Where V_R means the extrusion rate, ER means the extrusion ratio, D_B means the diameter of the sample before extrusion and D_E means the diameter of extruded bars after extrusion. In the current study. Since D_B, D_E, V_R and ER are all fixed, the extrusion strain rate mainly depends on the extrusion rate according to equation (3). As the extrusion rate increases, the extrusion strain rate $\dot{\varepsilon}$ gradually increases, which results in increasing the Z value and decreasing the $\overline{d}_{DRX}$. This is contradictory to the actual change in of Mg-2Zn-0.8Sr-0.2Ca alloys extruded at 200 °C&0.1 mm/s and 200 °C&1.0 mm/s. On the one hand, when the magnesium alloy is subjected to low-temperature extrusion, the lower the extrusion rate, the lower the critical stress required for DRX nucleation. This leads to a smaller nucleation resistance and a higher nucleation rate, contributing to the formation of fine DRXed grains. On the other hand, extrusion heat will inevitably occur during the extrusion, and the faster the extrusion speed, the higher the extrusion heat. This results in an increase in the actual temperature, which accelerates the growth of grains [24, 27, 28].

Figure 4 shows the TEM images of Mg-2Zn-0.8Sr-0.2Ca alloys. When the extrusion parameter was 200 °C&1.0 mm/s, the microstructure of the Mg-2Zn-0.8Sr-0.2Ca alloy was mainly comprised of equiaxed DRXed grains with some nano-sized precipitates (marked in yellow arrows in Figure 4(a)). As shown in Figure 4(b), when the extrusion speed declined to 0.1mm/s, the microstructure of the Mg-2Zn-0.8Sr-0.2Ca alloy extruded at 200 °C&0.1 mm/s consisted of a large number of undynamically recrystallized (unDRXed) regions and a few DRXed grains. There were plenty of dislocations accumulate in unDRXed regions. Furthermore, the volume fraction of unDRXed regions declined in the alloy (Figure 4(c)) relative to that extruded at 200 °C&0.1 mm/s.

To determine the composition of the precipitates in the Mg-2Zn-0.8Sr-0.2Ca alloys, TEM observation and selected area electron diffraction (SAED) were performed. Take the Mg-2Zn-0.8Sr-0.2Ca alloy extruded at 200 °C&0.1 mm/s for instance, Figure 5(a)(b) shows its bright-field image and the corresponding SAED. By combining the SAED pattern (Figure 5(b)), EDS results (Figure 2(e)) and XRD patterns (Figure 3), the compositions of the nano-sized precipitated phases was confirmed as $MgZn_2$ phase. According to the literature [29], the $MgZn_2$ phase has a hexagonal structure (where a=0.523nm; c=0.858nm), and there are a lot of $MgZn_2$ precipitates on the (0001) of a-Mg matrix. Some $MgZn_2$ phases and the a-Mg matrix have the following orientation relationship: $(0001)_{MgZn2}//(0001)_{a\text{-}Mg}$, $[11\text{-}20]_{MgZn2}//[10\text{-}10]_{a\text{-}Mg}$. The orientation relationship between the SAED of the precipitated phase and the SAED of the a-Mg matrix is in parallel for the present Mg-2Zn-0.8Sr-0.2Ca alloy. This indicated that the nano-sized precipitated $MgZn_2$ phase was highly coherent with the a-Mg matrix. Besides, it can be seen from the TEM images at higher magnification (Figure 5(c)) that high-density

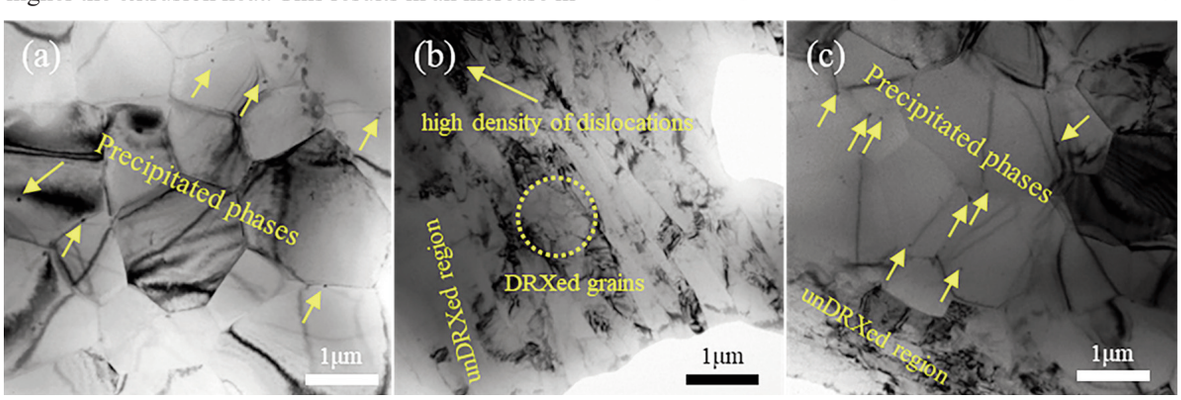

Figure 4. *TEM images of Mg-2Zn-0.8Sr-0.2Ca alloys extruded at different extrusion parameters: (a) 200°C&1.0mm/s, (b) 200°C&0.1mm/s and (c) 240°C&0.1mm/s*

dislocations were accumulated in unDRXed regions and plenty of dislocation lines existed in the Mg-2Zn-0.8Sr-0.2Ca alloys extruded at 200 °C&0.1 mm/s. Meanwhile, when the extrusion parameter was 200 °C&0.1 mm/s, a large number of twins appeared (Figure 5(c)), which could also lead to the accumulation of high-density dislocations at the twin grain boundaries [30, 31].

3.2. Texture of as-extruded Mg-2Zn-0.8Sr-0.2Ca alloy

Figure 6 shows the EBSD inverse pole figure (IPF) maps, the (0001) pole figures and the inverse pole figures of Mg-2Zn-0.8Sr-0.2Ca alloys along the ED. Besides, the grain boundary misorientation in the Fig. S1. and Fig. S2 were provided. It was further

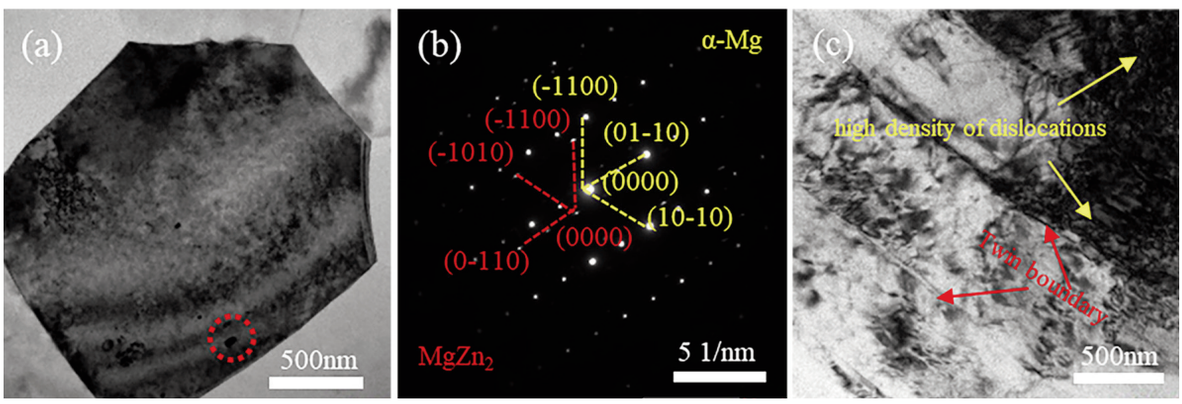

Figure 5. *(a)(b) TEM bright field images and corresponding SAED patterns of Mg-2Zn-0.8Sr-0.2Ca alloy extruded at 200°C&0.1mm/s; (c) TEM images for the unDRXed regions of Mg-2Zn-0.8Sr-0.2Ca alloys extruded at 200°C&0.1mm/s*

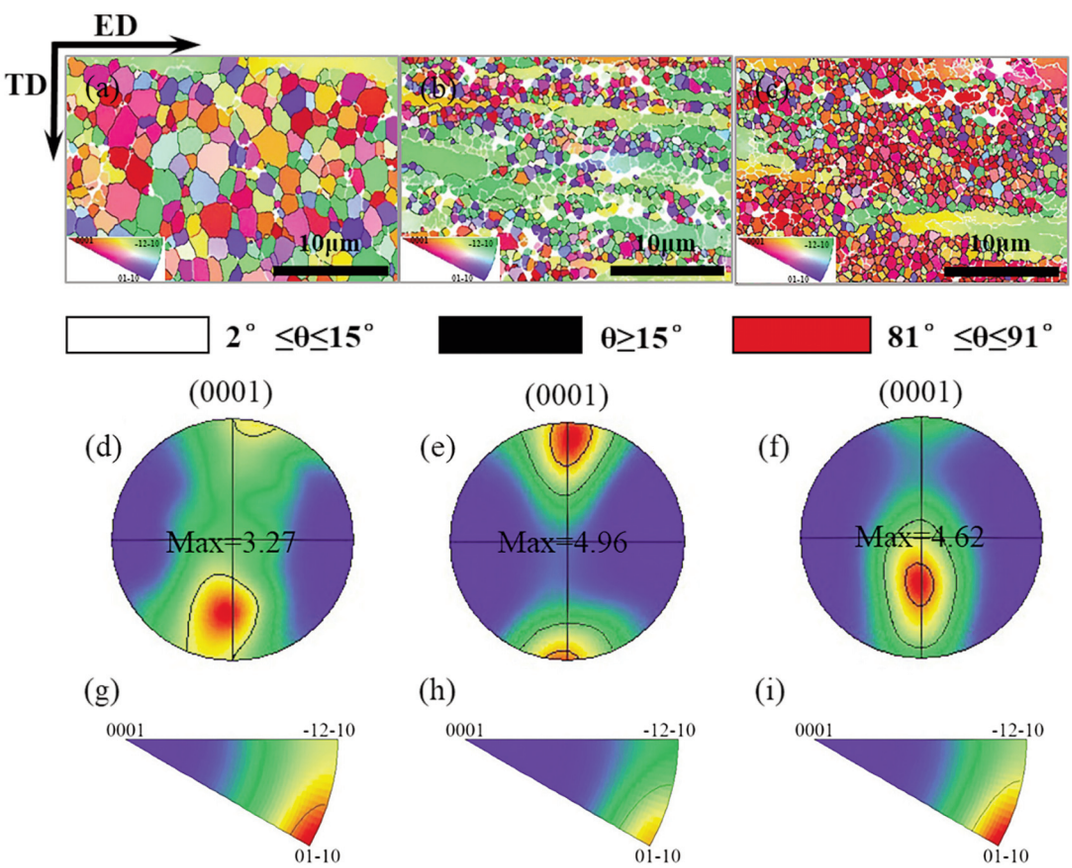

Figure 6. *EBSD inverse pole figure (IPF) maps, the (0001) pole figures and the inverse pole figures of Mg-2Zn-0.8Sr-0.2Ca alloys along the ED extruded at different extrusion parameters: (a)(d)(g) 200°C&1.0mm/s, (b)(e)(h) 200°C&0.1mm/s and (c)(f)(i) 240°C&0.1mm/s*

confirmed from the IPF maps (Figure 6(a)(b)(c)) that the obvious DRX occurred after extrusion, and the DRXed regions were composed of refined equiaxed grains with random orientation. In contrast, the large unDRXed grains in the unDRXed regions showed a significant preferred orientation. As the extrusion temperature and extrusion rate increased, the V_{DRX} and also increased, which was consistent with the light microscope observation. Besides, the small-angle grain boundaries were mostly concentrated near the coarse unDRXed grains. In comparison, the large-angle grain boundaries were mostly concentrated near the equiaxed DRXed grains. Besides, some {10-12} <10-11> extension twins with the misorientation angles of 86±5° existed in DRXed regions [32]. Due to the lower Schmid factor of {10-12} <10-11> extension twinning relative to {1-100} <11-20> cylindrical slip [33], DRX was difficult to occur, resulting in the formation of unDRXed regions. Figure 6(d)(e)(f) offers the (0001) pole figure of the extruded Mg-2Zn-0.8Sr-0.2Ca alloys and Figure 6(g)(h)(i) is the corresponding inverse pole figure. All Mg-2Zn-0.8Sr-0.2Ca alloys extruded at different parameters showed typical {0001} <10-10> basal textures. As the extrusion parameter was 200 °C&1.0mm/s, the basal texture intensity was 3.27 mud. The preferred orientation of the grains was mainly concentrated in the <01-10> component, while the orientations of some grains was distributed in the <-12-10> component. By decreasing the extrusion speed, the basal texture intensity increased to 4.96 mud. Further, with increasing the extrusion temperature to 240°C at 0.1mm/s, the basal texture intensity slightly decreased to 4.62 mud with <-12-10> orientation of some grains. This indicated that as the extrusion rate and extrusion temperature increased, the basal texture of the alloy gradually shifted from <01-10> component to <-12 -10> component, which was interrelated with the increase of the $\bar{d}_{DRX}$ as the extrusion rate and the extrusion temperature increased. The similar texture orientation shifted from {0002} <10-10> component to {0002} <11-20> component during grain growth in the rolled AZ31B [34].

Recent studies have shown [35, 36] that the basal texture intensity of as-extruded alloys is interrelated with the V_{DRX}, and the texture intensity of the unDRXed region is significantly higher than that of the DRXed region. Therefore, in order to further analyze the reasons for the difference in texture intensity, the DRXed regions and unDRXed regions under each extrusion process are analyzed, respectively.

Figure 7 shows the EBSD inverse pole figure (IPF) maps, (0001) pole figures and inverse pole figures of the DRXed regions of the Mg-2Zn-0.8Sr-0.2Ca alloys along the ED extruded at different extrusion parameters. Besides, the grain boundary misorientation in the Fig. S3 was provided. As the extrusion rate changed from 1.0mm/s to 0.1mm/s, V_{DRX} decreased from 93% to 60%, and the corresponding basal texture intensity increased from 2.74 mud to 3.37 mud. The preferred orientation of the grains in the inverse pole figure shifted from the <01-10> component and the <-12-10> component to the <01-10> component. This result was consistent with the work that the higher the value of V_{DRX}, the lower the texture intensity. When the extrusion rate was maintained at 0.1mm/s and the temperature was increased to 240°C, the V_{DRX} correspondingly increased from 60% to 73%. The basal texture intensity increased from 3.37 mud to 3.99 mud. In general, the higher the value of V_{DRX}, the lower the intensity of the texture. But the basal texture intensity was also affected by the precipitated phases. On the one hand, the precipitated phases could weaken the texture by promoting the occurrence of DRX. On the other hand, the precipitated phases could weaken the texture by pinning the grain boundary. In the as-extruded alloys, the density of vacancies at the grain boundary was high and the stored energy was enormous, which were the sites of preferential nucleation of the precipitated phases [37]. The finer the grain size, the more the total grain boundary area, which led to more potential nucleation sites for the precipitated phases to nucleate. As for the current Mg-2Zn-0.8Sr-0.2Ca alloy, the $\bar{d}_{DRX}$ increased with the rise of extrusion temperature, reducing the potential nucleation sites of the precipitated phases. Therefore, the volume fraction of the precipitated phase at 200°C&0.1 mm/s was higher than that at 240°C&0.1 mm/s which gave rise to the stronger ability to weaken the texture, resulting in a lower texture intensity at 200°C&0.1 mm/s.

Figure 8 (a)(b)(c) is the EBSD inverse pole figure (IPF) maps, (d)(e)(f) is the (0001) pole figures and (g)(h)(i) is the inverse pole figures of the unDRXed regions of the Mg-2Zn-0.8Sr-0.2Ca alloys along the ED. Besides, the grain boundary misorientation in the Fig. S4 was provided. The unDRXed regions presented a strong basal texture relative to the basal texture of the DRXed regions. This was because the grains in the unDRXed regions were coarse and the preferred orientation was more pronounced, resulting in higher texture intensity. At the same time, when the extrusion process was 200°C&1.0mm/s (Figure 8(a)(d)(g)), the volume fraction of unDRX was only 7% and the corresponding basal texture intensity was 14.43 mud, this ocurred because the poles in the pole figure were very concentrated, and the orientation of the grain was distributed in the <01-10> component in the inverse pole figure. Simultaneously, when the extrusion process was 200°C&0.1mm/s (Figure 8(b)(e)(h)), the volume fraction of unDRX was 40%,

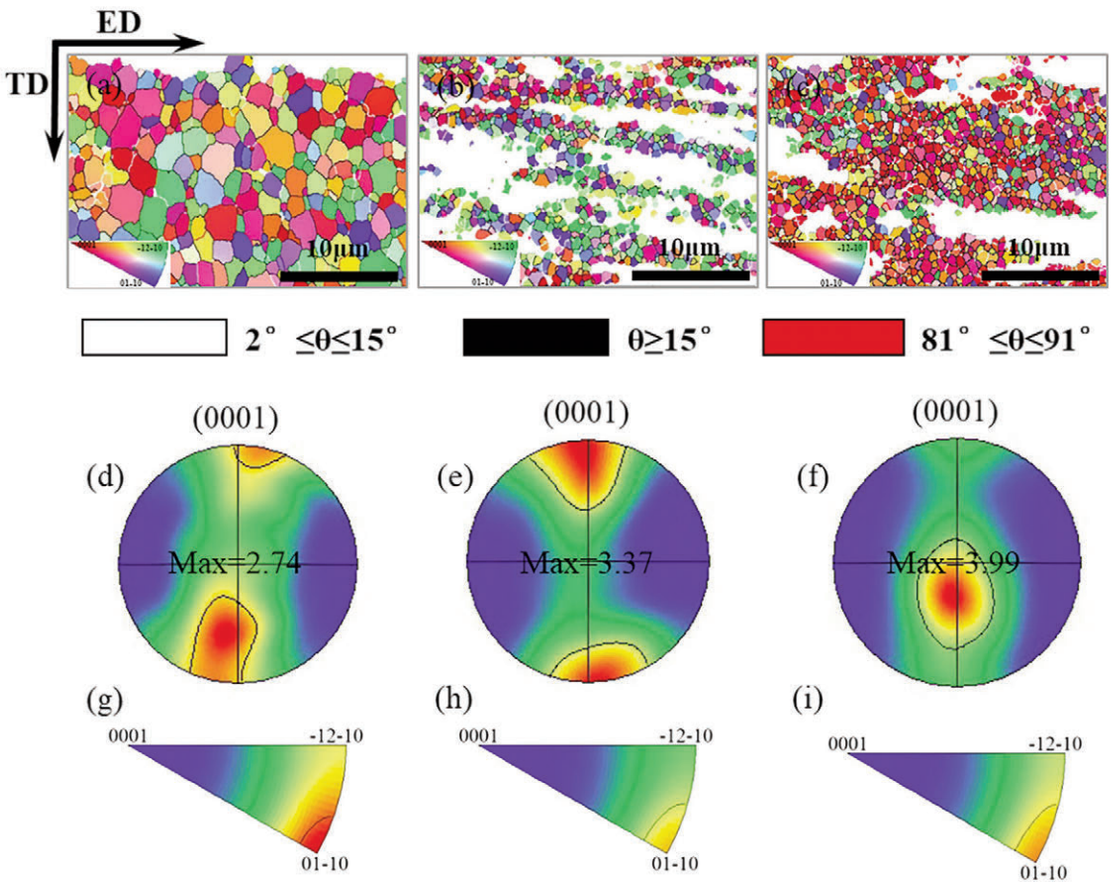

Figure 7. *EBSD inverse pole figure (IPF) maps, the (0001) pole figures and the inverse pole figures of the DRXed regions of Mg-2Zn-0.8Sr-0.2Ca alloys along the ED extruded at different extrusion parameters: (a)(d)(g) 200°C&1.0mm/s, (b)(e)(h) 200°C&0.1mm/s and (c)(f)(i) 240°C&0.1mm/s*

but the corresponding basal texture intensity was only 7.85 mud. This was because the poles in the pole figure were relatively scattered, and the grain orientation distribution in the inverse pole figure shifts from the <01-10> component to the <-12-10> component. Meanwhile, when the extrusion process was 240°C&0.1mm/s (Figure 8(c)(f)(i)), the volume fraction of unDRX was 27% and the corresponding basal texture intensity was 9.03 mud, this was because the poles in the pole figure were relatively concentrated, and the grain orientation in the inverse pole figure was mostly distributed in the <01-10> component, and there is less transition to the <-12-10> component.

Figure 9 depicts the changes in the grain orientation line profile in the DRXed region and unDRXed region of Mg-2Zn-0.8Sr-0.2Ca alloys after extrusion at 200°C&0.1 mm/s. Figure 9(b)(c) gives that on the AB straight line from the large deformation grains G1 to G5 in the unDRXed region, where the misorientation of large deformation grains varies from 0° to 13.3°. Figure 9(b)(d) shows that on the CD straight line from the large deformed grain G6 to the large deformed grain G10, the changes in the misorientation angle of the DRXed grains of G7, G8, G9, and G10 were 89.7°, 90.9°, 74.5°, and 41.6° respectively. This further revealed that the small-angle grain boundaries were mostly concentrated near the large deformed grains, while the large-angle grain boundaries were mainly concentrated near the equiaxed DRXed grains.

3.3. Mechanical properties

Figure 10(a) shows the engineering stress-strain curves of Mg-2Zn-0.8Sr-0.2Ca alloys extruded at different parameters and Figure 10(b) gives TYS, UTS and EL based on Figure 10(a) [20]. The corresponding values of TYS, UTS, and EL are gathered in Table 2. Fig. 10. (c) shows the strain hardening rate curves of the alloys. Figure 10(c) shows the strain hardening rate curve of the alloys, which is the typical stage III and IV strain hardening behavior in polycrystalline magnesium alloys. The TYS, UTS, and EL of the Mg-2Zn-0.8Sr-0.2Ca alloy after extrusion at 200°C&1.0 mm/s were 261.2 MPa, 271.3 MPa, and 15.3 %, respectively. When the

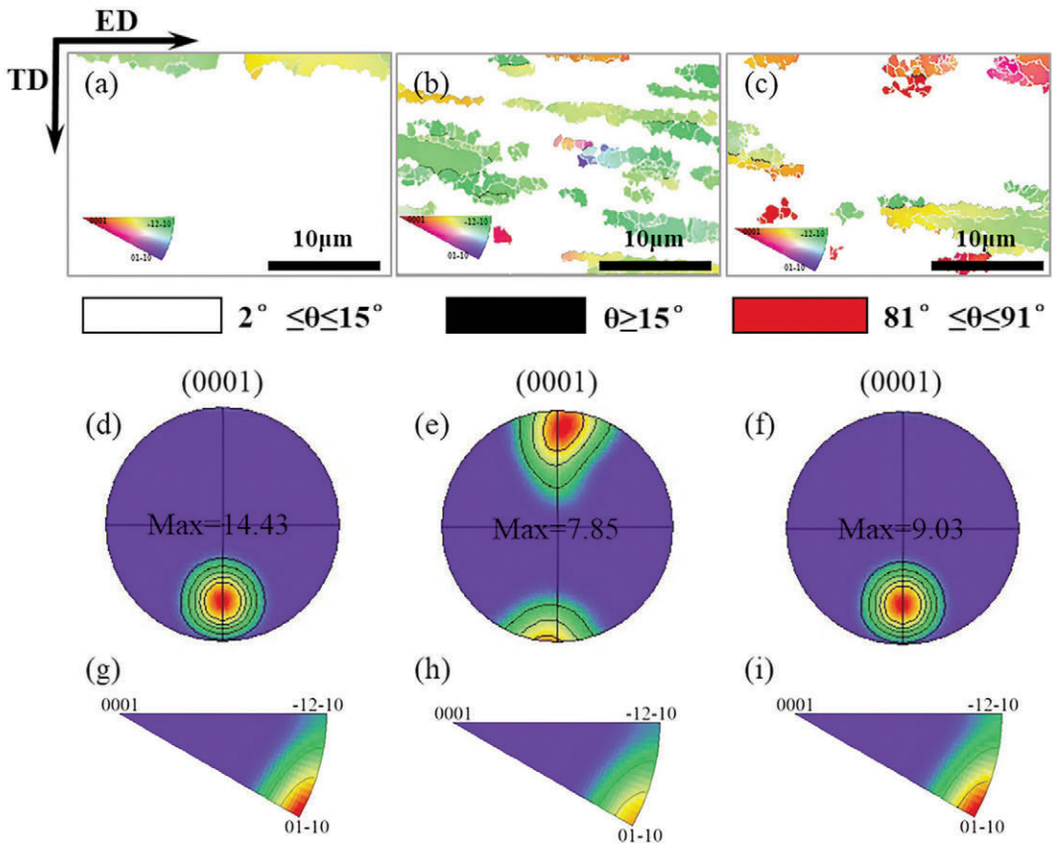

Figure 8. *EBSD inverse pole figure (IPF) maps, the (0001) pole figures and the inverse pole figures of the unDRXed regions of Mg-2Zn-0.8Sr-0.2Ca alloys along the ED extruded at different extrusion parameters: (a)(d)(g) 200°C&1.0mm/s, (b)(e)(h) 200°C&0.1mm/s and (c)(f)(i) 240°C&0.1mm/s*

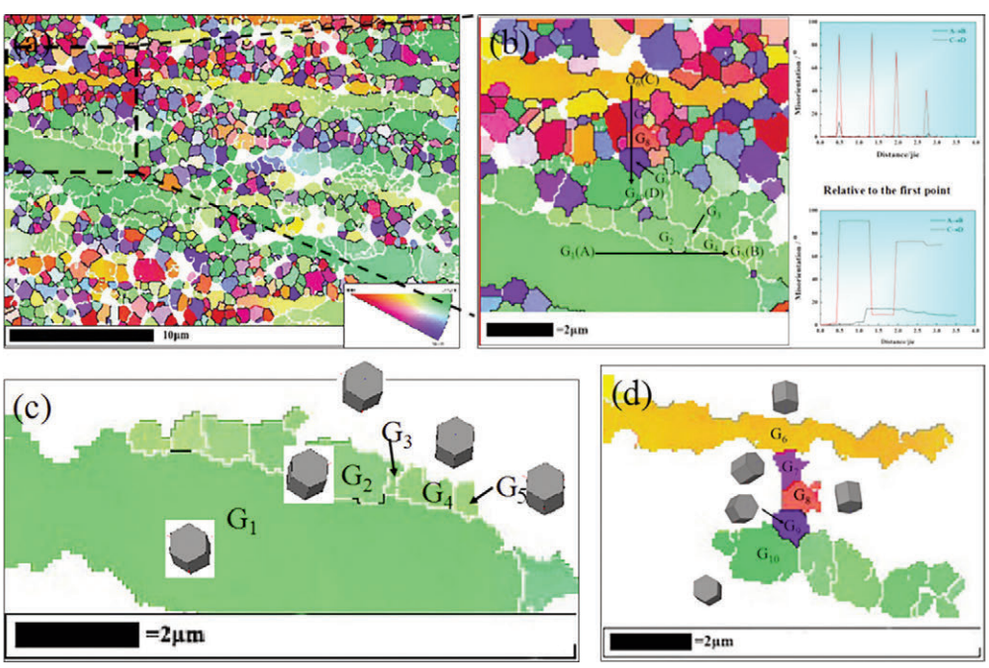

Figure 9. *Analysis of grain orientation for DRXed and unDRXed of Mg-2Zn-0.8Sr-0.2Ca alloy extruded at 200°C&0.1mm/s: (a) inverse pole figure map; (b) line profile of misorientation angle along AB and CD; (c) the distribution of grain in arrow AB; (d) the distribution of grain in arrow CD*

extrusion speed decreased to 0.1 mm/s, the YS, UTS, and EL were 393.1 MPa, 418.4 MPa, and 5.7%, respectively. While the extrusion rate was maintained at 0.1 mm/s and the extrusion temperature increased to 240°C, the YS, UTS, and EL were 339.9 MPa, 350.2 MPa, and 10.9 %, respectively. It can be seen that with the decline in extrusion temperature or rate, the YS and UTS of Mg-2Zn-0.8Sr-0.2Ca alloys increased while the EL decreased. The comparison in mechanical properties between as-extruded Mg-2Zn-0.8Sr-0.2Ca alloys and other Mg-Zn alloys are given in Figure 11 [14, 16, 21, 22, 38-42]. The results showed that the strength of Mg-2Zn-0.8Sr-0.2Ca alloy extruded at 200°C&0.1 mm/s was significantly higher than other Mg-Zn series extruded at higher temperature or faster speed, moreover, it was also superior to other AZ series alloys.

The main strengthening mechanisms for metal materials can be commonly owed to solid-solution strengthening, grain-boundary strengthening, dislocation strengthening, and precipitation strengthening [41]. In the current work, Zn, Ca, and Sr elements formed many second phase particles, which resulted in the Zn, Ca, and Sr elements not being completely dissolved in the Mg matrix. It can be roughly concluded that solid-solution strengthening provided a limited strengthening to the present extruded Mg-2Zn-0.8Sr-0.2Ca alloys.

As far as magnesium alloy was concerned, the microstructure after extrusion deformation was composed of equiaxed grains and large deformed regions. The grain-boundary strengthening could expressed by the Hall-Petch equation as [43]: $\sigma_y = \sigma_0 + kd^{(-1/2)}$.σ_0 is the friction stress of the material, which can be represented by the yield stress of 41 MPa of the as-homogenized Mg-2Zn-0.8Sr-0.2Ca alloys [23], k is the material constant, and d is the grain size. Generally, the grains of the unDRXed regions were coarse, so the influence of the unDRXed region on grain-boundary strengthening was ignored in the current work. Therefore, the yield stress of Mg-2Zn-0.8Sr-0.2Ca alloys under different extrusion processes could expressed as [24, 43]:

$$\sigma_{gb,DRX} = f_{DRX} k d_{as-extruded}^{-\frac{1}{2}} \quad (4)$$

where $\sigma_{gb,DRX}$ means the yield stress of DRXed regions, and k is a material constant. In the current work, k was set to 217 MPa μm$^{1/2}$ [16], f_{DRX} meant the volume fraction of the DRX and d meant the average grain size of the DRXed grains. It can be calculated that the contribution of grain-boundary strengthening to the yield stress of Mg-2Zn-0.8Sr-0.2Ca alloys at three different extrusion processes was 173.1MPa, 178.8MPa, and 181.7MPa, respectively.

Generally speaking, the dislocation density in magnesium alloys is very different in the DRXed and unDRXed regions. The nucleation process of DRX is a process that consumes dislocations, so the dislocation density in DRXed regions is much lower, as shown in Figure 4. Thus, the influence of the DRXed regions on dislocation strengthening was ignored in the current work. Therefore, the dislocation strengthening to the contribution of the yield stress can be expressed by the following equation [24, 44]:

$$\sigma_{dislocation,unDRX} = f_{unDRX} M \alpha G b \sqrt{\rho} \quad (5)$$

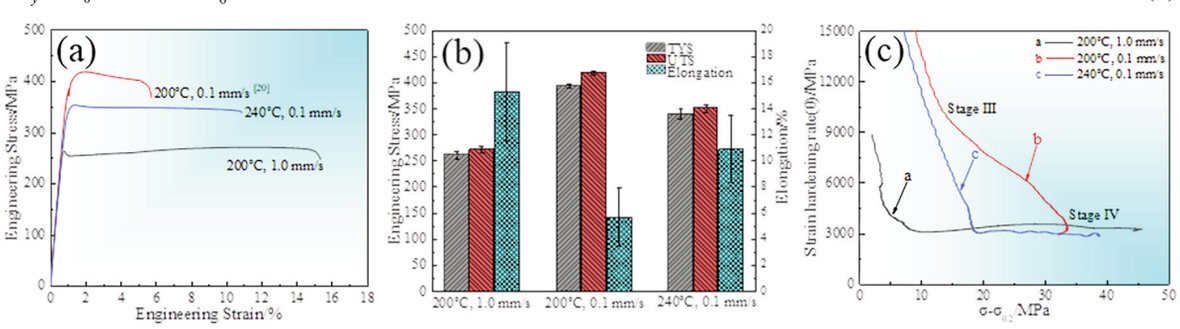

Figure 10. *(a) The tensile stress-strain curves [20], (b) tensile strength and (c) strain hardening rate curves of the Mg-2Zn-0.8Sr-0.2Ca alloys extruded at different extrusion parameters*

Table 2. *The mechanical properties of Mg-2Zn-0.8Sr-0.2Ca alloys extruded at different extrusion parameters*

Materials	Condition	TYS (MPa)	UTS (MPa)	Elongation (%)	References
Mg-2Zn-0.8Sr-0.2Ca (wt.%)	200°C,1.0mm/s	261.2±6.7	271.3±6.5	15.3±3.8	This study
Mg-2Zn-0.8Sr-0.2Ca (wt.%)	200°C,0.1mm/s	393.1±4.0	418.4±4.2	5.7±2.2	This study
Mg-2Zn-0.8Sr-0.2Ca (wt.%)	240°C,0.1mm/s	340.0±9.9	350.2±6.8	10.9±2.6	This study

where f_{unDRX} means the volume fraction of unDRX; M means the Taylor factor related to texture intensity and the M value is usually 2-5. The effect of texture on stress is related to the slip of dislocations. The higher the texture strength is, the more difficult the dislocation slip is to be activated, which results in higher stress. In this work, the value of M is 3.5 [44]. a is a constant (0.2); G means the shear modulus (16.6 GPa); b means the Berber vector (0.32 nm); ρ means the dislocation density, which is difficult to determine. The dislocation density is about 10^{15}-10^{16} m^{-2} in the unDRXed region of the metal material with larger deformation [24], so it was reasonable to take the dislocation density as 5×10^{15} m^{-2} in this work. It can be calculated that the contribution of dislocation strengthening to the yield stress of Mg-2Zn-0.8Sr-0.2Ca alloys under three different processes was 18.4MPa, 105.2MPa, and 71.0MPa, respectively.

Besides, it can be seen from Figure 2, Figure 4, and Figure 5 that there were some nano-sized precipitated phases in the extruded Mg-2Zn-0.8Sr-0.2Ca alloys, which was a significant barrier preventing dislocation migration during plastic deformation. When dislocations migrated to the precipitated phases, dislocation loops were formed around the precipitated phases, which was beneficial to improve the material's strength. Therefore, for the extruded Mg-2Zn-0.8Sr-0.2Ca alloys, the contribution of precipitation strengthening to the yield stress can be expressed by the following equation [24]:

$$\Delta\tau_p = \frac{Gb}{2\pi\sqrt{1-\gamma}\left(\frac{0.779}{\sqrt{f}}-0.785\right)d_p} ln\frac{0.785d_p}{b} \quad (6)$$

where d_p means the average size of the precipitated phases, g means the Poisson's ratio (0.35) and f means the volume fraction of the precipitated phases, G means the shear modulus (16.6 GPa); b means the Berber vector (0.32 nm). Due to the small number of precipitated phases, the quantitative calculation could not be carried out in the current work. It can be calculated that the solid-solution strengthening to the yield stress of Mg-2Zn-0.8Sr-0.2Ca alloys at three different extrusion processes was 15.7%, 10.4%, and 12.1%, respectively, the contribution of grain-boundary strengthening to the yield stress of Mg-2Zn-0.8Sr-0.2Ca alloys at three different extrusion processes was 66.3%, 45.5% and 53.4%, respectively, and the contribution of dislocation strengthening to the yield stress of Mg-2Zn-0.8Sr-0.2Ca alloys under three different processes was 7.0%, 26.8% and 20.9%, respectively. In summary, different hot extrusion processes had significant effects on the mechanical properties of Mg-2Zn-0.8Sr-0.2Ca alloys. When the DRX was complete, the grain refinement strengthening had a more substantial impact on the material's yield stress. However, when the material had more unDRXed regions, the effect of dislocation strengthening in the unDRXed regions on the material's yield stress increased significantly. Besides, the yield stress was also affected by precipitation phases.

Figure 12 shows the light microscope image of the near fracture surface and the SEM image of the fracture surface of the Mg-2Zn-0.8Sr-0.2Ca alloys after extrusion in different processes. It can be found from the comparison of Figure 12 (a)(d) and (b)(e) that when the extrusion temperature remained the same and the extrusion rate dropped from 1.0 mm/s to 0.1 mm/s, the number of twins near the fracture surface increased, the dimples in the fracture surface were gradually reduced and tear ridges appeared, which revealed that the fracture forms of the extruded Mg-2Zn-0.8Sr-0.2Ca alloys changed from ductile fracture to brittle fracture, and the EL decreased from 15.3% to 5.7%. At the same time, it

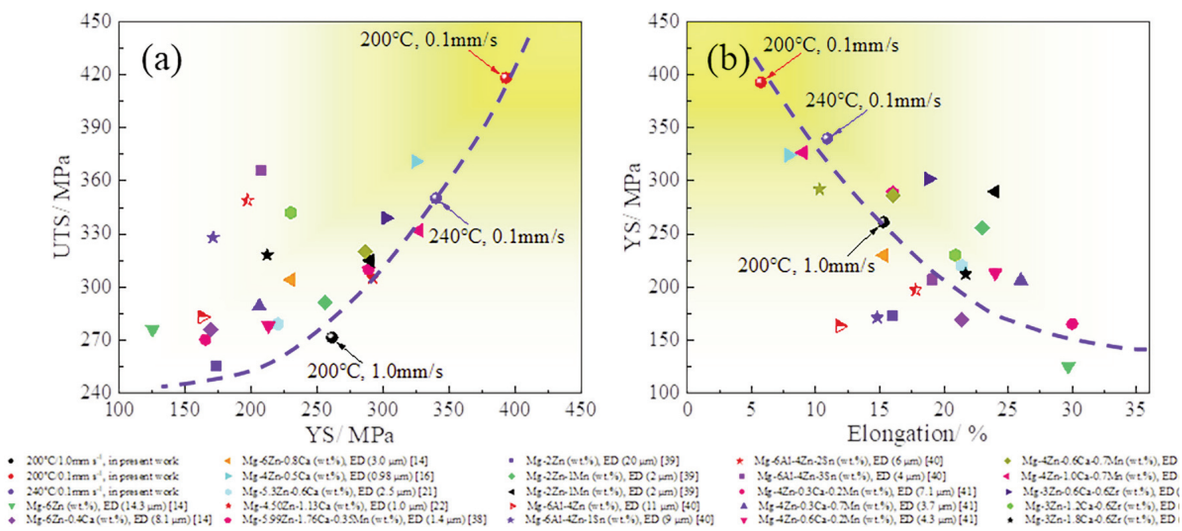

Figure 11. *Comparison of the mechanical properties between present as-extruded Mg-2Zn-0.8Sr-0.2Ca alloys and reported materials: (a) ultimate tensile strength vs. yield strength, (b) yield strength vs. elongation*

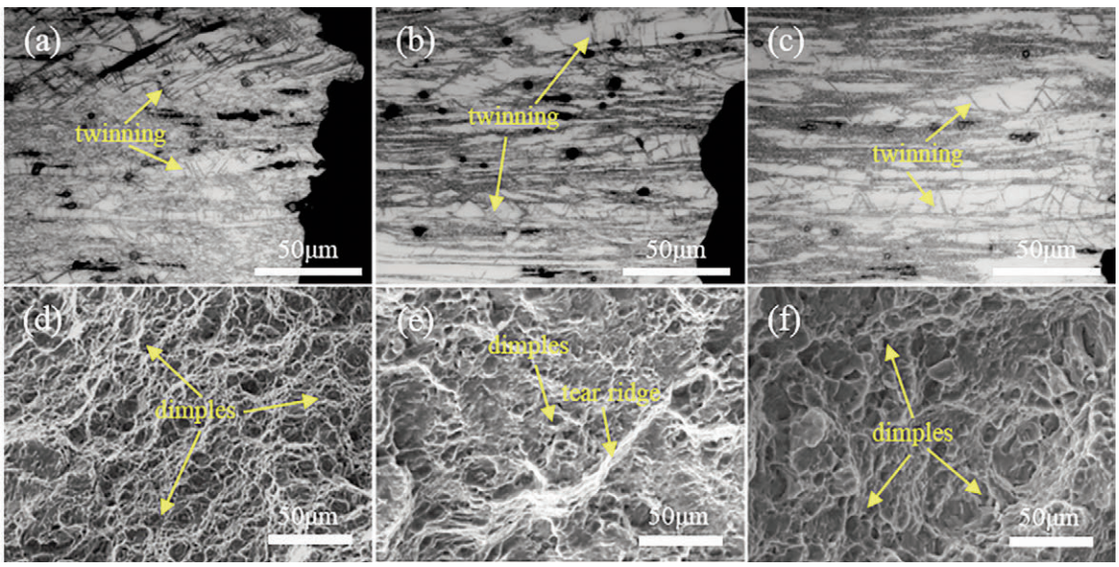

Figure 12. *The light microscope images and SEM micrographs of fractured tensile specimens of Mg-2Zn-0.8Sr-0.2Ca alloys extruded at different extrusion parameters: (a)(d) 200℃&1.0mm/s, (b)(e) 200℃&0.1mm/s and (c)(f) 240℃&0.1mm/s*

can be found from the comparison of Figure 12 (b)(e) and (c)(f) that when the extrusion rate was maintained at 0.1mm/s and the extrusion temperature was increased from 200°C to 240°C, the number of twins in the near fracture surface of the extruded Mg-2Zn-0.8Sr-0.2Ca alloy decreased, and there was no particularly pronounced tear ridge in the fracture surface, and the number of dimples increased significantly. Thus, the fracture forms of Mg-2Zn-0.8Sr-0.2Ca alloys changed from brittle fracture to mixture fracture, which resulted in the EL increase from 5.7% to 10.9%.

4. Conclusion

In the current work, Mg-2Zn-0.8Sr-0.2Ca alloys were extruded under different hot extrusion processes at 200℃&0.1mm/s, 200℃&1.0mm/s, and 240℃&0.1mm/s, respectively. The influence of extrusion parameters on the microstructure, texture and mechanical properties of Mg-2Zn-0.8Sr-0.2Ca (wt.%) alloy was systematically investigated. The main conclusions are summarized as follows:

(1) A large number of equiaxed grains appeared in the microstructure of the extruded Mg-2Zn-0.8Sr-0.2Ca alloy, and the grain size was significantly refined. With the increase of extrusion rate and extrusion temperature, the V_{DRX} and the gradually increased.

(2) Simultaneously, the broken second phases during the extrusion processes were $Ca_2Mg_6Zn_3$ and $Mg_{17}Sr_2$. Besides, some nano-sized $MgZn_2$ precipitates were dynamically precipitated during the extrusion process.

(3) With the decrease of extrusion rate and temperature, the texture intensity of the basal (0001) increased, and the maximum texture intensity of the basal (0001) was 4.96 mud at 200°C&0.1 mm/s. Besides, the texture intensity of the DRXed region was not only closely related to the volume fraction of the DRX but also significantly affected by the precipitated phases. The texture intensity of the unDRXed region was not only extremely interrelated with the degree of the unDRX but also closely related to the degree of dispersion of the poles.

(4) With the increase of extrusion temperature and extrusion rate, the YS and UTS gradually decreased, but the EL increased significantly. The Mg-2Zn-0.8Sr-0.2Ca alloy extruded at 200°C&0.1mm/s exhibited excellent mechanical properties with the YS of 393.1 MPa, UTS of 418.4 MPa, and EL of 5.7%. This was mainly attributed to the combined effects of grain-boundary strengthening, dislocation strengthening, and precipitation strengthening.

Acknowledgment

This work was supported by the National Natural Science Foundation of China [grant numbers 51771129, 51401144, 51771128]; the Program for the Outstanding Innovative Teams of Higher Learning Institutions of Shanxi; the Natural Science Foundation of Shanxi Province [grant numbers 2015021067 and 201601D011034]; and the Projects of International Cooperation in Shanxi [Grant no. 201703D421039].

Author's contributions statement

An Yang: Data collection, data interpretation, analysis, drafting, revision, and approval of the final

manuscript. Kai-bo Nie: Concept and design of the study, revision, approval of the final manuscript. Kun-Kun Deng: Revision, approval of the final manuscript. Jun-gang Han: Data collection, and approval of the final manuscript. Tao Xiao: Revision, and approval of the final manuscript. Xiuzhu Han: Revision, approval of the final manuscript.

Data availability

The raw/processed data required to reproduce these findings cannot be shared at this time due to technical or time limitations.

Conflicts of interest

The authors declare no conflicts of interest or personal relationships that could have appeared to influence the work reported in this paper.

References

[1] Z.R. Zeng, N. Stanford, C. H. J. Davies, J.F. Nie, N. Birbilis, Magnesium extrusion alloys: a review of developments and prospects, International Materials Reviews, 64(1) (2018) 27-62. https://doi.org/10.1080/09506608.2017.1421439

[2] K.K. Alaneme, E.A. Okotete, Enhancing plastic deformability of Mg and its alloys-A review of traditional and nascent developments, Journal of Magnesium and Alloys, 5(4) (2017) 460-475. https://doi.org/10.1016/j.jma.2017.11.001

[3] Y.W. Wang, J. You, A.G. Wang, J.P. Peng, Y.Z. Di, Production of Mg-Li alloys by aluminothermic vacuum reduction, Journal of Mining and Metallurgy, Section B: Metallurgy, 56(1) (2020) 43-49. https://doi.org/10.2298/JMMB190419053W

[4] H. Somekawa, A. Kinoshita, A. Kato, Effect of alloying elements on room temperature stretch formability in Mg alloys, Materials Science and Engineering: A, 732 (2018) 21-28. https://doi.org/10.1016/j.msea.2018.06.098

[5] K. Oh-ishi, R. Watanabe, C.L. Mendis, K. Hono, Age-hardening response of Mg-0.3 at.% Ca alloys with different Zn contents, Materials Science and Engineering: A, 526(1-2) (2009) 177-184. https://doi.org/10.1016/j.msea.2009.07.027

[6] Y. Shi, X.Q. Liu, Z.L. Liu, H.J. Xie, Y. H. Wang, J. Li, Effect of Zn content on corrosion behavior of Mg-Y-Zn alloys, Journal of Mining and Metallurgy, Section B: Metallurgy, 58(1) (2022) 51-61. https://doi.org/10.2298/JMMB210525048S

[7] D.Y. Maeng, T.S. Kim, J.H. Lee, S.J. Hong, S.K. Seo, B.S. Chun, Microstructure and strength of rapidly solidified and extruded Mg-Zn alloys, Scripta Materialia, 43(5) (2000) 385-389. https://doi.org/10.1016/S1359-6462(00)00428-0

[8] X. Gao, J.F. Nie, Characterization of strengthening precipitate phases in a Mg-Zn alloy, Scripta Materialia, 56(8) (2007) 645-648. https://doi.org/10.1016/j.scriptamat.2007.01.006

[9] X. Meng, Z. Jiang, S. Zhu, S. Guan, Effects of Sr addition on microstructure, mechanical and corrosion properties of biodegradable Mg-Zn-Ca alloy, Journal of Alloys and Compounds, 838 (2020) 155611. https://doi.org/10.1016/j.jallcom.2020.155611

[10] T.V. Larionova, W.W. Park, B.S. You, A ternary phase observed in rapidly solidified Mg-Ca-Zn alloys, Scripta Materialia, 45(1) (2001) 7-12. https://doi.org/10.1016/S1359-6462(01)00982-4

[11] X. G. Liu, X. D. Peng, W. D. Xie, Q. Y. Wei, Preparation technologies and applications of strontium-magnesium master alloys, Materials Science Forum, 488-489 (2005) 31-34. https://doi.org/10.4028/www.scientific.net/MSF.488-489.31

[12] R. Guan, A.F. Cipriano, Z. Zhao, J. Lock, D. Tie, T. Zhao, T. Cui, H. Liu, Development and evaluation of a magnesium-zinc-strontium alloy for biomedical application-Alloy processing, microstructure, mechanical properties, and biodegradation, Materials Science and Engineering: C, 33(7) (2013) 3661-3669. https://doi.org/10.1016/j.msec.2013.04.054

[13] T. Ding, H. Yan, J. Chen, W. Xia, B. Su, Z. Yu, Dynamic recrystallization and mechanical properties of high-strain-rate hot rolled Mg-5Zn alloys with addition of Ca and Sr, Transactions of Nonferrous Metals Society of China, 29(8) (2019) 1631-1640. https://doi.org/10.1016/s1003-6326(19)65070-3

[14] Y.Z. Du, X.G. Qiao, M.Y. Zheng, D.B. Wang, K. Wu, I.S. Golovin, Effect of microalloying with Ca on the microstructure and mechanical properties of Mg-6 mass% Zn alloys, Materials & Design, 98 (2016) 285-293. https://doi.org/10.1016/j.matdes.2016.03.025

[15] Y. Liu, D. Liu, Y. Zhao, M. Chen, Corrosion degradation behavior of Mg-Ca alloy with high Ca content in SBF, Transactions of Nonferrous Metals Society of China, 25(10) (2015) 3339-3347. https://doi.org/10.1016/S1003-6326(15)63968-1

[16] W.J. Li, K.K. Deng, X. Zhang, K.B. Nie, F.J. Xu, Effect of ultra-slow extrusion speed on the microstructure and mechanical properties of Mg-4Zn-0.5Ca alloy, Materials Science and Engineering: A, 677 (2016) 367-375. https://doi.org/10.1016/j.msea.2016.09.059

[17] K.B. Nie, Z.H. Zhu, P. Munroe, K.K. Deng, J.G. Han, The effect of Zn/Ca ratio on the microstructure, texture and mechanical properties of dilute Mg-Zn-Ca-Mn alloys that exhibit superior strength, Journal of Materials Science, 55(8) (2019) 3588-3604. https://doi.org/10.1007/s10853-019-04174-4

[18] M.G. Zhou, X.S. Huang, Y. Morisada, H. Fujii, Y. Chino, Effects of Ca and Sr additions on microstructure, mechanical properties, and ignition temperature of hot-rolled Mg-Zn alloy, Materials Science and Engineering A, 769 (2020) 138474. https://doi.org/10.1016/j.msea.2019.138474

[19] J.S. Wei, S.N. Jiang, Z.Y. Chen, C.M. Liu, Increasing strength and ductility of a Mg-9Al alloy by dynamic precipitation assisted grain refinement during multi-directional forging. Materials Science and Engineering: A, 780 (2020) 139192. https://doi.org/10.1016/j.msea.2020.139192

[20] J.H. Zhang, K.B. Nie, K.K. Deng, J.G. Han, J.Y. Yi, Ultrahigh strength TiC_{np}/Mg-2Zn-0.8Sr-0.2Ca magnesium matrix composite processed by combining multidirectional forging with extrusion, Composites Communications, 27 (2021) 100847. https://doi.org/10.1016/j.coco.2021.100847

[21] L.B. Tong, M.Y. Zheng, L.R. Cheng, D.P. Zhang, S. Kamado, J. Meng, H.J. Zhang, Influence of deformation rate on microstructure, texture and mechanical properties of indirect-extruded Mg-Zn-Ca alloy, Materials Characterization, 104 (2015) 66-72. https://doi.org/10.1016/j.matchar.2014.09.020

[22] Y.Z. Du, M.Y. Zheng, C. Xu, X.G. Qiao, K. Wu, X.D. Liu, G.J. Wang, X.Y. Lv, Microstructures and mechanical properties of as-cast and as-extruded Mg-4.50Zn-1.13Ca (wt%) alloys, Materials Science and Engineering: A, 576 (2013) 6-13. https://doi.org/10.1016/j.msea.2013.03.034

[23] K.B. Nie, J.G. Han, K.K. Deng, Z.H. Zhu, Simultaneous improvements in tensile strength and elongation of a Mg-2Zn-0.8Sr-0.2Ca alloy by a combination of microalloying and low content of TiC nanoparticles, Materials Letters, 260 (2020) 126951. https://doi.org/10.1016/j.matlet.2019.126951

[24] X.K. Kang, K.B. Nie, K.K. Deng, Y.C. Guo, Effect of extrusion parameters on microstructure, texture and mechanical properties of Mg-1.38Zn-0.17Y-0.12Ca (at.%) alloy, Materials Characterization, 151 (2019) 137-145. https://doi.org/10.1016/j.matchar.2019.03.004

[25] S.K. Chamoli, S. Singh, C.L. Guo, Metal-Dielectric-Metal metamaterial-based ultrafast hydrogen sensors in the water transmission window, IEEE Sensors Letters, 4(5) (2020) 3500904. https://doi.org/10.1109/lsens.2020.2991081

[26] R.K. Koju, Y. Mishin, Atomistic study of grain-boundary segregation and grain-boundary diffusion in Al-Mg alloys, Acta Materialia, 201 (2020) 596-603. https://doi.org/10.1016/j.actamat.2020.10.029

[27] S.H. Park, B.S. You, R.K. Mishra, A.K. Sachdev, Effects of extrusion parameters on the microstructure and mechanical properties of Mg-Zn-(Mn)-Ce/Gd alloys, Materials Science and Engineering: A, 598 (2014) 396-406. http://doi.org/10.1016/j.msea.2014.01.051

[28] S.S. Park, B.S. You, D.J. Yoon, Effect of the extrusion conditions on the texture and mechanical properties of indirect-extruded Mg-3Al-1Zn alloy, Journal of Materials Processing Technology, 209(18-19) (2009) 5940-5943. https://doi.org/10.1016/j.jmatprotec.2009.07.012

[29] X. Gao, J.F. Nie, Characterization of strengthening precipitate phases in a Mg-Zn alloy, Scripta Materialia, 56(8) (2007) 645-648. https://doi.org/10.1016/j.scriptamat.2007.01.006

[30] A. Zhang, R. Kang, L. Wu, H. Pan, H. Xie, Q. Huang, Y. Liu, Z. Ai, L. Ma, Y. Ren, G. Qin, A new rare-earth-free Mg-Sn-Ca-Mn wrought alloy with ultra-high strength and good ductility, Materials Science and Engineering: A, 754 (2019) 269-274. https://doi.org/10.1016/j.msea.2019.03.095

[31] H. Pan, G. Qin, Y. Huang, Y. Ren, X. Sha, X. Han, Z. Liu, C. Li, X. Wu, H. Chen, C. He, L. Chai, Y. Wang, J. Nie, Development of low-alloyed and rare-earth-free magnesium alloys having ultra-high strength, Acta Materialia, 149 (2018) 350-363. https://doi.org/10.1016/j.actamat.2018.03.002

[32] R.D. Doherty, D.A. Hughes, F.J. Humphreys, J.J. Jonas, D.J. Jensen, M.E. Kassner, W.E. King, T.R. McNelley, H.J. McQueen, A.D. Rollett, Current issues in recrystallization: a review, Materials Science and Engineering: A, 238(2) (1997) 219-274. https://doi.org/10.1016/S0921-5093(97)00424-3

[33] S.W. Xu, K. Oh-ishi, S. Kamado, T. Homma, Twins, recrystallization and texture evolution of a Mg-5.99Zn-1.76Ca-0.35Mn (wt.%) alloy during indirect extrusion process, Scripta Materialia, 65(10) (2011) 875-878. https://doi.org/10.1016/j.scriptamat.2011.07.053

[34] M.A. Steiner, J.J. Bhattacharyya, S.R. Agnew, The origin and enhancement of {0001} <112¯0> texture during heat treatment of rolled AZ31B magnesium alloys, Acta Materialia, 95 (2015) 443-455. https://doi.org/10.1016/j.actamat.2015.04.043

[35] X. Jin, W. Xu, Z. Yang, C. Yuan, D. Shan, B. Teng, B.C. Jin, Analysis of abnormal texture formation and strengthening mechanism in an extruded Mg-Gd-Y-Zn-Zr alloy, Journal of Materials Science & Technology, 45 (2020) 133-145. https://doi.org/10.1016/j.jmst.2019.11.021

[36] M.G. Jiang, C. Xu, H. Yan, G.H. Fan, T. Nakata, C.S. Lao, R.S. Chen, S. Kamado, E.H. Han, B.H. Lu, Unveiling the formation of basal texture variations based on twinning and dynamic recrystallization in AZ31 magnesium alloy during extrusion, Acta Materialia, 157 (2018) 53-71. https://doi.org/10.1016/j.actamat.2018.07.014

[37] J.F. Nie, Effects of precipitate shape and orientation on dispersion strengthening in magnesium alloys, Scripta Materialia, 48(8) (2003) 1009-1015. https://doi.org/10.1016/S1359-6462(02)00497-9

[38] S.W. Xu, K. Oh-ishi, H. Sunohara, S. Kamado, Extruded Mg-Zn-Ca-Mn alloys with low yield anisotropy, Materials Science and Engineering: A, 558 (2012) 356-365. https://doi.org/10.1016/j.msea.2012.08.012

[39] J. She, P. Peng, L. Xiao, A.T. Tang, Y. Wang, F.S. Pan, Development of high strength and ductility in Mg-2Zn extruded alloy by high content Mn-alloying, Materials Science and Engineering: A, 765 (2019) 138203. https://doi.org/10.1016/j.msea.2019.138203

[40] X.Y. Wang, Y.F. Wang, C. Wang, S. Xu, J. Rong, Z.Z. Yang, J.G. Wang, H.Y. Wang, A simultaneous improvement of both strength and ductility by Sn addition in as-extruded Mg-6Al-4Zn alloy, Journal of Materials Science & Technology, 49 (2020) 117-125. https://doi.org/10.1016/j.jmst.2019.04.048.

[41] C.Q. Liu, X.H. Chen, J. Chen, A. Atrens, F.S. Pan, The effects of Ca and Mn on the microstructure, texture and mechanical properties of Mg-4Zn alloy, Journal of Magnesium and Alloys, 9(3) (2020) 1084-1097. https://doi.org/10.1016/j.jma.2020.03.012

[42] B.N. Wang, F. Wang, Z. Wang, L. Zhou, Z. Liu, P.L. Mao, Microstructure and mechanical properties of Mg-Zn-Ca-Zr alloy fabricated by hot extrusion-shearing process, Materials Science and Engineering: A, 795 (2020) 139937. https://doi.org/10.1016/j.msea.2020.139937

[43] H. Yu, Y. Xin, M. Wang, Q. Liu, Hall-Petch relationship in Mg alloys: A review. Journal of Materials Science & Technology, 34(2) (2018) 248-256. https://doi.org/10.1016/j.jmst.2017.07.022

[44] K.B. Nie, Z.H. Zhu, P. Munroe, K.K. Deng, J.G. Han, Microstructure, Tensile Properties and Work Hardening Behavior of an Extruded Mg-Zn-Ca-Mn Magnesium Alloy, Acta Metallurgica Sinica (English Letters), 33 (2020) 922-936. https://doi.org/10.1007/s40195-020-01061-9.

Appendix

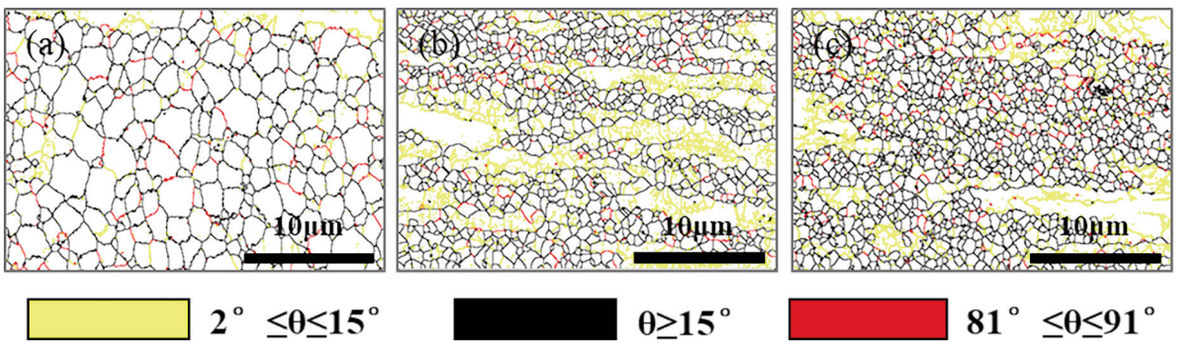

Figure S1. *The grain boundary orientation EBSD maps of Mg-2Zn-0.8Sr-0.2Ca alloys along the ED extruded at different extrusion parameters: (a) 200° C&1.0mm/s, (b) 200° C&0.1mm/s and (c) 240° C&0.1mm/s*

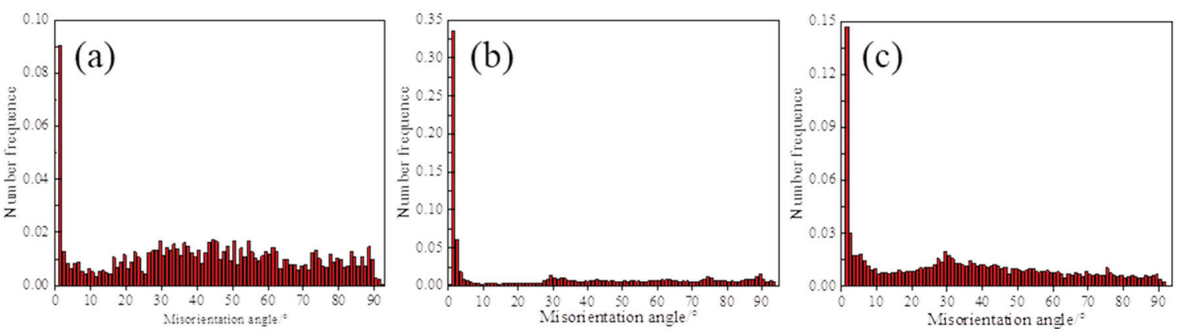

Figure S2. *The misorientation angle distribution maps of Mg-2Zn-0.8Sr-0.2Ca alloys along the ED extruded at different extrusion parameters: (a) 200° C&1.0mm/s, (b) 200° C&0.1mm/s and (c) 240° C&0.1mm/s*

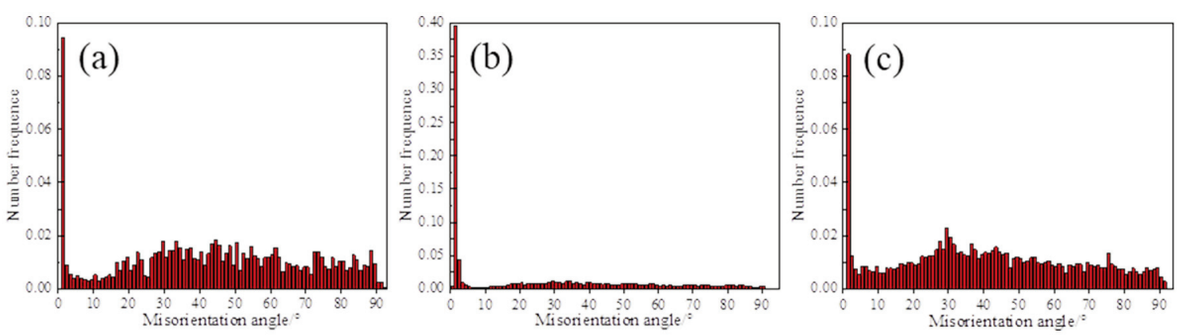

Figure S3. *The misorientation angle distribution maps of the DRXed regions of Mg-2Zn-0.8Sr-0.2Ca alloys along the ED extruded at different extrusion parameters: (a) 200° C&1.0mm/s, (b) 200° C&0.1mm/s and (c) 240° C&0.1mm/s*

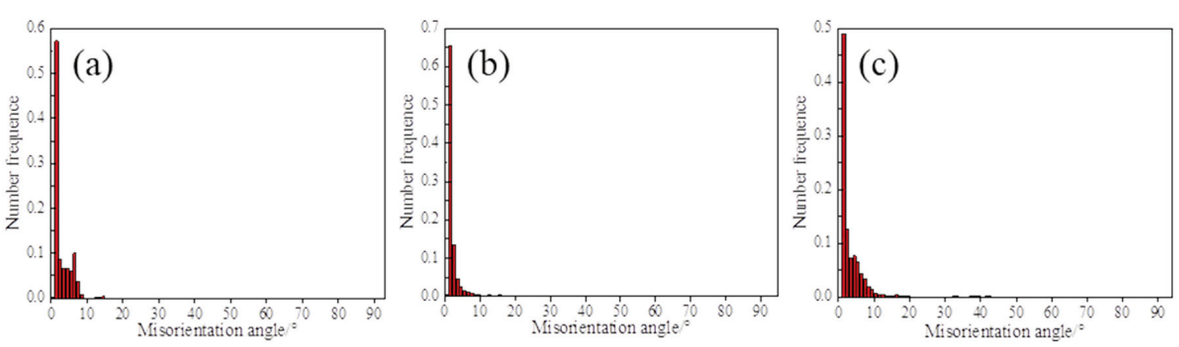

Figure S4. *The misorientation angle distribution maps of the unDRXed regions of Mg-2Zn-0.8Sr-0.2Ca alloys along the ED extruded at different extrusion parameters: (a) 200° C&1.0mm/s, (b) 200° C&0.1mm/s and (c) 240° C&0.1mm/s*

MIKROSTRUKTURA I ZATEZNA SVOJSTVA Mg-2Zn-0.8Sr-0.2Ca LEGURE EKSTRUDIRANE NA NISKOJ TEMPERATURI PRI MALOJ BRZINI

A. Yang [a], K.-B. Nie [a, b, *], K.-K. Deng [a, b], J.-G. Han [a], T. Xiao [c], X.-Z. Han [c,]**

[a] Fakultet za nauku o metrijalima, Tehnološki univerzitet u Taijuanu, Taijuan, NR Kina
[b] Glavna laboratorija za napredne materijale na bazi magnezijuma u Šanksi provinciji, Tehnološki univerzitet u Taijuanu, Taijuan, NR Kina
[c] Institut za sistemsko inženjerstvo za svemirske letelice u Pekingu, Peking, NR Kina

Apstrakt

U ovom radu je predstavljen postupak podvrgavanja ekstruziji Mg-2Zn-0.8Sr-0.2Ca legure na relativno niskim temperaturama (240 i 200°C) pri malim brzinama (1.0 mm/s i 0.1 mm/s). Prosečna veličina i zapreminski udeo rekristalisanih zrna u ekstrudiranoj leguri postepeno su opadali sa smanjenjem brzine ili temperature ekstruzije. U leguri Mg-2Zn-0.8Sr-0.2Ca su se pojavile određene druge faze, $Ca_2Mg_6Zn_3$ i $Mg_{17}Sr_2$, zajedno sa precipitiranim fazama $MgZn_2$ nano veličine. Zapreminski udeo $MgZn_2$ faze u leguri se postepeno povećavao kako su se brzina ili temperatura ekstruzije smanjivale. Dobijena granica razvlačenja je iznosila 393,1 MPa, granična zatezna čvrstoća 418,4 MPa i izduženje od 5,7% za Mg-2Zn-0.8Sr-0.2Ca ekstrudiranu leguru na 200°C i 0.1 mm/s. Glavni mehanizam ojačavanja se može pripisati graničnom, dislokacijskom i taložnom ojačanju, koja su se dogodila zbog promene veličine zrna, pojave drugih faza i bazalne strukture ekstrudirane Mg-2Zn-0.8Sr-0.2Ca legure.

Ključne reči: *Mg-2Zn-0.8Sr-0.2Ca legura; Ektruzija; Mikrostruktura; Tekstura; Mehanička svojstva*